Evolution of a line vortex in stratified flow

Surupa Shaw and John P. McHugh*
The Department of Mechanical Engineering, The University of New Hampshire, Durham, New Hampshire 03824, USA

(Received 10 April 2018; published 12 June 2019)

A distributed vortex in a stratified fluid is treated using numerical simulations in two dimensions. The distributed vortex allows the density field and velocity field to evolve together, as happens in real flows behind lifting surfaces. The numerical simulations treat the anelastic equations using a spectral method in space with periodic horizontal directions and a projection method in time using the third-order Adams-Bashforth method. The primary parameter is the Froude number. For large Froude number, the distributed vorticity quickly rolls up and forms a vortex pair, approximately matching cases initiated as a fully developed vortex pair. For small Froude number, the vortices disintegrate into internal waves. The results indicate that the transition Froude number with a distributed vortex is larger than cases initiated with a vortex pair.

DOI: 10.1103/PhysRevFluids.4.064803

I. INTRODUCTION

Numerical results by Garten *et al.* [1] show that a vortex pair released in a stratified fluid will disintegrate into internal waves if the Froude number is in the flow regime where buoyancy dominates, with Froude number defined as

$$F_r = \frac{W_0}{b_0 N}. \tag{1}$$

Here W_0 is the velocity that one vortex induces at the center of the other, b_0 is the vortex spacing, and N is the buoyancy frequency. They suggest $F_r < 1$ is the buoyancy-dominated regime. For $F_r > 1$, where flow is dominated by advection, they report that the vortex pair propagates vertically in a manner similar to the case of constant-density flow.

One important application of the dynamics of a vortex pair is the flow behind a finite length wing or other surface that generates side force. The existence of a trailing vortex wake behind wings has been known since the early days of flight and is first mentioned by Prandtl [2], who included a trailing vortex sheet in his original calculation of wing lift using lifting line theory. Many subsequent studies have considered the vortex wake of commercial aircraft, as reviewed by Spalart [3], Rossow [4], Gerz *et al.* [5], and Paoli and Shariff [6]. It is now generally accepted that the flow in the near wake of a wing has shed vorticity distributed across the span of the wing, while the flow in the far wake is more like a pair of discrete vortices [7]. The transition from distributed vorticity (near wake) to vortex pair (far wake) is referred to as vortex roll-up.

Attempts to understand the roll-up process in constant density flow started with Kaden [8] and Betz [29]. Betz used the Kutta-Joukowsky theorem to treat a wide variety of cases, including the case of a symmetric wing that is pertinent here. Since these early efforts, similar but more sophisticated theories have been considered by Spreiter and Sacks [9], Moore and Saffman [10], Bilanen and Donaldson [11], and Chadwick and Rahulan [12].

Extensive results using numerical simulation confirms this roll-up pattern; see, for example, Czech *et al.* [13], who treat flow over an airplane in three dimensions using the constant-density

*Corresponding author: john.mchugh@unh.edu

equations. Numerical simulations of the entire wake, including the near wake and the far wake, are difficult. This practical matter has led many researchers to focus on the far wake using a vortex pair as the starting point, including the work of Garten *et al.* [1].

Stratification has been included only in limited cases, such as Saffman [14]. Saffman's results extend the previous theoretical results of Turner [15], both treating greatly simplified models of the behavior of the vortices. An important feature highlighted by Saffman is that a vortex pair traps a finite volume of fluid and causes this volume to propagate vertically. Since the fluid is stratified, this volume of fluid experiences a buoyant force acting to restore the volume to its original position. Ultimately this buoyancy is important for predicting the vertical position of the vortex wake.

Examples in the literature of numerical simulations in a stratified fluid initiated with a vortex pair include Garten *et al.* [1], Hill [16], Spalart [17], Robins and Delisi [18], Holzapfel and Gerz [19], and Nomura *et al.* [20]. The common approach is to impose the static vertical density profile, usually chosen to be the profile that corresponds to constant Brunt-Vaisala frequency, and initiate the velocity field with a pair of laminar vortices.

This previous work has shown that the density field inside a stratified vortex quickly becomes mixed. Wave motion is initiated during the early stages of motion, before mixing erases the stratification within the vortex. If wave making is not initiated early, then it will not occur, e.g., if the stratification within the vortex core was initially uniform, then the flow would again proceed without significant internal waves, even if the Froude number (determined with N outside the vortex) is very small. Hence the manner of initiation of the vortex pair is important to the final behavior, and initiating the flow with the velocity field of a vortex pair along with the vertically stratified density field inside the vortex is not consistent with the roll-up process that occurs behind a wing.

Also evident in previous numerical simulations is that the vortices in a vortex pair drift together in stratified flow. Garten *et al.* [1] argue that this drift is due to the baroclinic torque that each vortex experiences as a result of vorticity creation at the edge of the vortices. Crow [21] also reports this vorticity creation. Ravichandran *et al.* [22] treat the merging of two counterrotating vortices, starting with constant density inside the vortices and different constant density outside. They show a dramatic change in enstrophy shortly after merger. Ravichandran *et al.* do not consider the instability treated here, since they initiate the motion as constant density: the wave-making regime of Garten *et al.* [1] occurs only when flow is initially stratified inside the vortices.

Recently, Ortiz *et al.* [23] treated perturbations to a vortex pair in a stratified flow, assuming weak stratification and a quasisteady base flow. They computed a two-dimensional flow without noise, then a linear three-dimensional flow with added noise. Growth rates were extracted from the three-dimensional case after subtracting the two-dimensional flow, all at a single value of time. They find unstable symmetric modes at small wave number that correspond to the Crow instability [21] and antisymmetric unstable modes at larger wave number (short-wave). These short-wave unstable modes dominate the Crow instability and perhaps explain the puffs that are sometimes visible in contrails. The calculations of Ortiz *et al.* were performed at relatively high Froude numbers, $2 \leqslant F_r \leqslant 10$, and thus do not address the lower Froude number instability treated below.

Here the flow is treated with the initial vorticity distributed in a line, a more realistic model of the near wake. With a line vortex, the velocity and density fields evolve together during the roll-up process. Results are obtained with numerical simulations of the viscous Navier-Stokes equations. The wing load distribution is assumed to be constant, matching that of a delta wing. Results obtained with distributed vorticity are compared to that of a vortex pair, assuming the same circulation for each half.

At large Froude number with distributed initial vorticity, the effect of inertia is weakened when compared to a vortex pair, suggesting a higher Froude number (ratio of inertial to gravitational effects) for the same transition. Indeed, the results show that the distributed vortex delays to a larger Froude number the transition from buoyancy-dominated flow to advection-dominated flow. It is difficult to determine this Froude number precisely with repeated numerical simulations, but the transition value appears to be approximately $F_r \approx 2$ when the vorticity is initially distributed with constant load.

The largest commercial jets flying at cruise altitudes will have Froude numbers in the range $2 < F_r < 7$ approximately, mostly outside the range of the instability discussed here. Smaller aircraft will have smaller Froude numbers, and the present results are directly applicable. Other lifting surfaces, such as wind turbine blades, also have smaller Froude numbers and likely experience the instability discussed here.

II. THE GOVERNING EQUATIONS

The governing equations are the Navier-Stokes, continuity, energy, and state equations for a compressible gas. The approximate form used here are the anelastic equations [24]

$$\frac{D\vec{v}}{Dt} = -\nabla p^* + g\frac{\theta}{\bar{\theta}}\vec{k} + \nu\nabla^2\vec{v}, \tag{2}$$

$$\nabla\cdot(\bar{\rho}\vec{v}) = 0, \tag{3}$$

$$\frac{D\theta}{Dt} + w\frac{d\bar{\theta}}{dz} = \kappa\nabla^2\theta, \tag{4}$$

where $\vec{v}$ is the velocity, w is the vertical velocity component, θ is the potential temperature, $\bar{\theta}$ is the background profile of potential temperature, $\bar{\rho}$ is the background density profile, ν is the kinematic viscosity, and κ is the thermal diffusivity. The quantity p^* is defined by

$$p^* = c_p\bar{\theta}\left(\frac{p}{p_0}\right)^{\frac{R}{c_p}}, \tag{5}$$

where p is the pressure, c_p is the specific heat, R is the ideal gas constant, and p_0 is a reference pressure. This anelastic model eliminates compressible flow effects while retaining the large vertical change in density that occurs in the atmosphere. While the anelastic effects are retained here, for the parameter values used here the phenomena could be modeled adequately with the Boussinesq equations as well.

It is convenient to introduce buoyancy b:

$$b = g\frac{\theta}{\bar{\theta}}. \tag{6}$$

The energy equation (4) becomes

$$\frac{Db}{Dt} + N^2\left(1+\frac{b}{g}\right)w = \kappa\left\{\nabla^2 b - \frac{2}{g}N^2\frac{\partial b}{\partial z} + \left[\frac{N^4}{g^2} - \frac{1}{g}\frac{\partial}{\partial z}(N^2)\right]b\right\}, \tag{7}$$

where N is the buoyancy frequency,

$$N^2 = \frac{g}{\bar{\theta}}\frac{d\bar{\theta}}{dz}. \tag{8}$$

The extra diffusion terms that appear after substitution of the buoyancy are neglected, as they do not have much effect. The final energy equation is

$$\frac{Db}{Dt} + N^2\left(1+\frac{b}{g}\right)w = \kappa\nabla^2 b. \tag{9}$$

We make the equations dimensionless using a length scale L and velocity scale U, to be chosen later. The buoyancy is rescaled with the quantity N^2L. The dimensionless equations are

$$\frac{D\vec{v}}{Dt} = -\nabla p + \frac{1}{F_r^2}b\vec{k} + \frac{1}{R_e}\nabla^2\vec{v}, \tag{10}$$

$$\frac{Db}{Dt} + \left(1+\frac{R}{C_p}\frac{1}{H}\right)w = \frac{1}{R_eP_r}\nabla^2 b, \tag{11}$$

$$\nabla\cdot\vec{v} - \frac{1}{H}w = 0, \tag{12}$$

where

$$R_e = \frac{UL}{\nu}, \tag{13}$$

$$F_r = \frac{U}{LN}, \tag{14}$$

$$P_r = \frac{\nu}{\kappa}, \tag{15}$$

$$\frac{1}{H} = -L\frac{\overline{\rho}_z}{\overline{\rho}}. \tag{16}$$

An important quantity in the discussion that follows is the vorticity η,

$$\eta = w_x - u_z. \tag{17}$$

Taking the curl of the momentum equations results in the well-known vorticity equation, which for the present configuration is

$$\frac{D\eta}{Dt} = \frac{1}{F_r^2}\frac{\partial b}{\partial x} + \frac{1}{R_e}\nabla^2\eta. \tag{18}$$

The spatial discretization uses a Fourier transform in the horizontal with 256 coefficients, and Chebyshev-Gauss-Lobatto collocation in the vertical with 256 grid points [25]. Higher resolution with several cases showed no significant change in results.

The temporal integration is a projection method, similar to that of Karniadakis *et al.* [26], along with explicit integration of the momentum and energy equations, similar to that of Slinn and Riley [27]. Here the third-order Adams-Bashforth method is employed, which has minimal artificial damping of internal waves. The first step determines an intermediate velocity field $\vec{v}^*$:

$$\begin{aligned}\vec{v}^* - \vec{v}^n = \Bigg\{ &\frac{23}{12}\left[-(\vec{v}\cdot\boldsymbol{\nabla})\vec{v} - b\vec{k} + \frac{1}{R_e}\nabla^2\vec{v}\right]^n - \frac{16}{12}\left[-(\vec{v}\cdot\boldsymbol{\nabla})\vec{v} - b\vec{k} + \frac{1}{R_e}\nabla^2\vec{v}\right]^{n-1} \\ &+ \frac{5}{12}\left[-(\vec{v}\cdot\boldsymbol{\nabla})\vec{v} - b\vec{k} + \frac{1}{R_e}\nabla^2\vec{v}\right]^{n-2}\Bigg\}\Delta t.\end{aligned} \tag{19}$$

The velocity at the leading time step $\vec{v}^{n+1}$ and the pressure are related to this intermediate velocity by

$$\vec{v}^{n+1} - \vec{v}^* = -\boldsymbol{\nabla} p \Delta t. \tag{20}$$

The pressure is determined using

$$\nabla^2 p - \frac{1}{H}\frac{\partial p}{\partial z} = \frac{1}{\Delta t}\left[\boldsymbol{\nabla}\cdot\vec{v}^* + \frac{1}{H}w^*\right], \tag{21}$$

with the normal derivative of pressure set to zero on top and bottom. The buoyancy is advanced using

$$\begin{aligned}b^{n+1} - b^n = \Bigg\{ &\frac{23}{12}\left[-[\vec{v}\cdot\boldsymbol{\nabla}]b - \left(1 + \frac{R}{c_p}\frac{1}{H}b\right)w + \frac{1}{R_e P_r}\nabla^2 b\right]^n \\ &- \frac{16}{12}\left[-[\vec{v}\cdot\boldsymbol{\nabla}]b - \left(1 + \frac{R}{c_p}\frac{1}{H}b\right)w + \frac{1}{R_e P_r}\nabla^2 b\right]^{n-1} \\ &+ \frac{5}{12}\left[-(\vec{v}\cdot\boldsymbol{\nabla})b - \left(1 + \frac{R}{c_p}\frac{1}{H}b\right)w + \frac{1}{R_e P_r}\nabla^2 b\right]^{n-2}\Bigg\}\Delta t.\end{aligned} \tag{22}$$

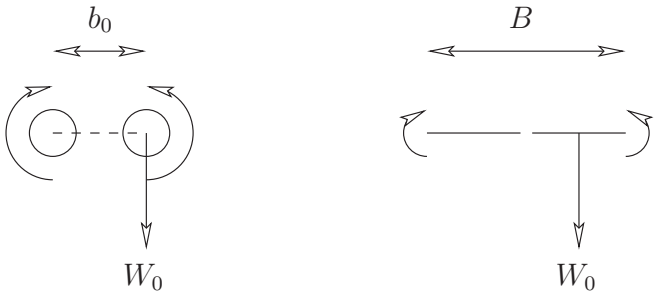

FIG. 1. Sketch of the initial conditions, both the vortex pair (left) and the line vortex (right). The downward velocity vector indicates the velocity of the right vortex induced by the left. The left vortex has the same downward velocity (not shown).

The presence of stratification causes a cascade of energy to scales of motion that are beneath the resolution of the present simulations. This cascade results in an accumulation of energy at the smallest resolved scale. With the present spectral method, this effect causes the last Fourier coefficient to grow monotonically with time. This growth of the last resolved scale is purely a computational artifact that does not significantly influence the motion, but must be controlled for practical reasons, and hence all variables are filtered at each time step.

The filter that is used here is the sequence of spectral filters discussed by Vandeven [28]. The filter is defined by

$$\omega(\zeta) = \sum_{q=1}^{p} \frac{(2p-1)!}{(p-1)!(2p-q)!} \zeta^{q-1}(1-\zeta)^{2p-q}, \tag{23}$$

where ω is the filter value and ζ is a dummy variable for the frequency. Vandeven [28] showed that spectral accuracy is retained with this filter family.

All results given below were achieved with $p = 15$, and R_e was set at 2500. Overall, the results given below are insensitive to the value R_e. Other parameter values are $P_r = 1$ and $H = 286$, approximately matching that of the atmosphere.

III. INITIAL CONDITIONS

The flow is initiated to approximately model the flow immediately behind a wing where the vorticity is still distributed across the wing and the fluid is vertically stratified. Such cases will be compared to the flow initiated traditionally using a vortex pair. For the vortex pair, two Gaussian vortices with opposite sense are placed at the same vertical position, spaced horizontally the distance b_0 (not to be confused with the buoyancy b). This configuration is shown in the sketch in Fig. 1 (left diagram).

The vortex line is achieved with a sequence of Gaussian vortices, equally spaced along a horizontal line of length B, the span. A range of the number of vortices M was considered, and it was found that the velocity field with $M \geqslant 300$ was adequately smooth with the chosen resolution. Values of M as large as 10 000 were treated with no significant difference in the final results.

The span of the distributed vortex B is chosen to match the spacing of the discrete vortex pair b_0 in the manner suggested by Betz [29]. Betz showed that the first moment of the final rolled-up vortex is equal to the moment of each half of the distributed vorticity. For the constant vorticity distribution chosen here,

$$B = 2b_0;$$

e.g., the distributed vortex is twice as long as the vortex pair spacing. Furthermore, the strength of the trailing vorticity is constant, except the sign is chosen to be positive for the right side of the

vortex line and negative for the left side. This configuration is also shown in the sketch in Fig. 1 (right diagram)

The length scale is now chosen to be the vortex pair spacing, $L = b_0$, and the velocity scale is chosen to be the induced velocity, $U = W_0$. The velocity field for the vortex pair is

$$u = -\frac{z - z_0}{(x - x_0)^2 + (z - z_0)^2}\left[1 - e^{-\frac{(x-x_0)^2+(z-z_0)^2}{2\sigma^2}}\right]\left[\frac{1}{1 - e^{-\frac{1}{2\sigma^2}}}\right] + \frac{z - z_0}{(x + x_0)^2 + (z - z_0)^2}\left[1 - e^{-\frac{(x+x_0)^2+(z-z_0)^2}{2\sigma^2}}\right]\left[\frac{1}{1 - e^{-\frac{1}{2\sigma^2}}}\right], \tag{24}$$

$$w = \frac{x - x_0}{(x - x_0)^2 + (z - z_0)^2}\left[1 - e^{-\frac{(x-x_0)^2+(z-z_0)^2}{2\sigma^2}}\right]\left[\frac{1}{1 - e^{-\frac{1}{2\sigma^2}}}\right] - \frac{x + x_0}{(x + x_0)^2 + (z - z_0)^2}\left[1 - e^{-\frac{(x+x_0)^2+(z-z_0)^2}{2\sigma^2}}\right]\left[\frac{1}{1 - e^{-\frac{1}{2\sigma^2}}}\right], \tag{25}$$

where $x_0 = 1/2$, z_0 are the initial vortex positions. The value of σ sets the size of the core of each vortex. The value $\sigma = 0.125$ is chosen here, matching that of Garten *et al.* [1].

The velocity field for the line vortex is

$$u = -\sum_{j=1}^{M}\Gamma_j \frac{z - z_j}{(x - x_j)^2 + (z - z_j)^2}\left[1 - e^{-\frac{(x-x_j)^2+(z-z_j)^2}{2\sigma^2}}\right], \tag{26}$$

$$w = \sum_{j=1}^{M}\Gamma_j \frac{x - x_j}{(x - x_j)^2 + (z - z_j)^2}\left[1 - e^{-\frac{(x-x_j)^2+(z-z_j)^2}{2\sigma^2}}\right], \tag{27}$$

with

$$x_j = \left(2\frac{j-1}{M-1} - 1\right),$$

$$z_j = z_0.$$

The strength of the individual vortices is chosen to be constant, $\Gamma_j = \Gamma_1$, and chosen so that the distributed vortex has the same circulation as the vortex pair. This is achieved by choosing the induced velocity due to one-half of the distributed vortex to be equal to induced velocity of an isolated Gaussian vortex W_0:

$$\Gamma_1 = \frac{\left[1 - e^{-\frac{1}{2\sigma^2}}\right]}{\sum_{j=1}^{M/2}\left[\frac{1}{\frac{1}{2}+\frac{2j-1}{M-1}}\right]\left[1 - e^{-\frac{1}{2\sigma^2}\left(\frac{1}{2}+\frac{2j-1}{M-1}\right)^2}\right]}. \tag{28}$$

As discussed in Phillips [30], a distributed vortex will roll up and form a core flow. This core flow is modeled approximately with the mature Gaussian vortex with $\sigma = 0.125$. For the distributed vortex, the core is allowed to form by choosing a much smaller value of σ for the individual vortices. This value was found by treating a sequence of smaller values of σ until the simulation results no longer depend on σ, resulting in the value $\sigma = 0.001$.

IV. RESULTS

Simulations initiated with a distributed vortex will be compared directly to simulations initiated with a vortex pair in what follows. Throughout the discussion, reference to a "line vortex" implies a simulation that is initiated with distributed vorticity using the initial velocity field given by (26)

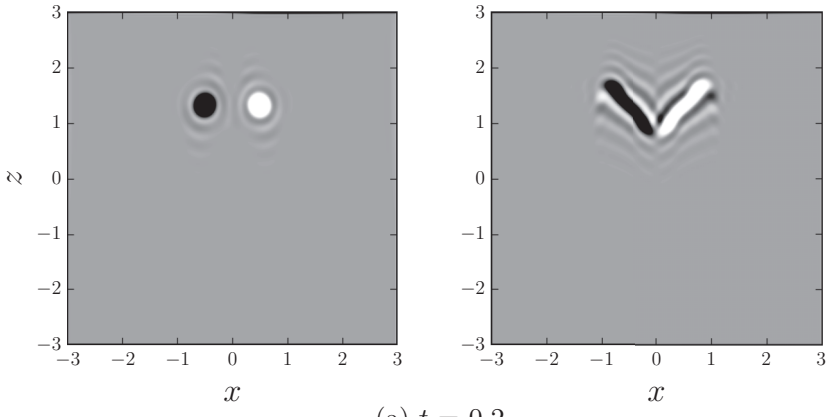

(a) $t = 0.2$

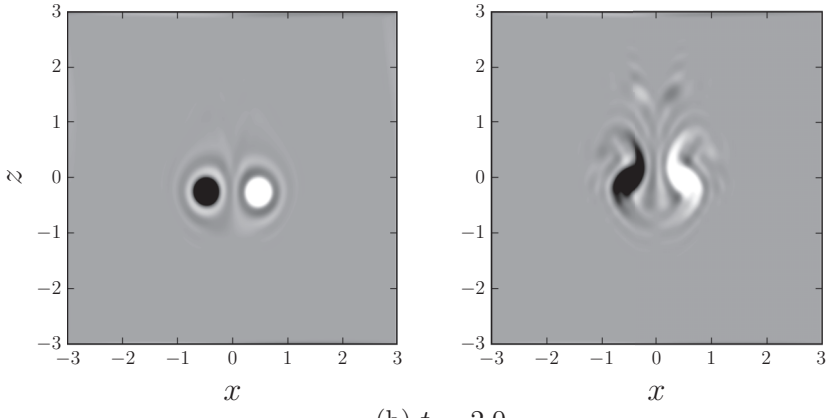

(b) $t = 2.0$

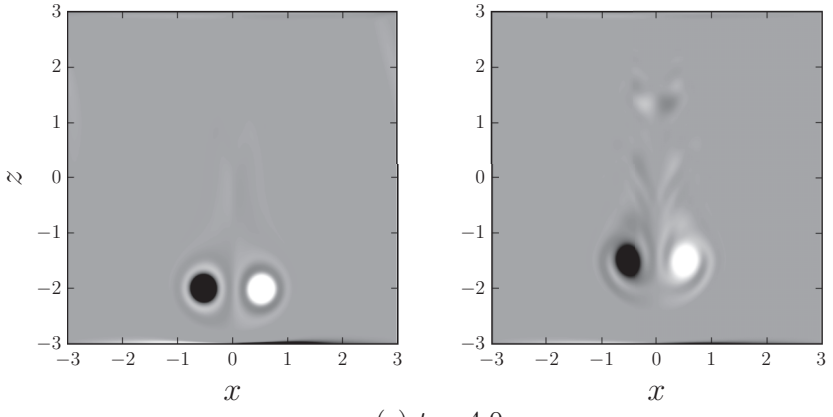

(c) $t = 4.0$

FIG. 2. Contours of vorticity for the vortex pair (left) and the line vortex (right) with constant density. Background gray is zero vorticity, while dark means positive and light means negative vorticity. There are 200 contour levels evenly distributed over the vorticity interval of $-10 \geqslant \eta \geqslant 10$.

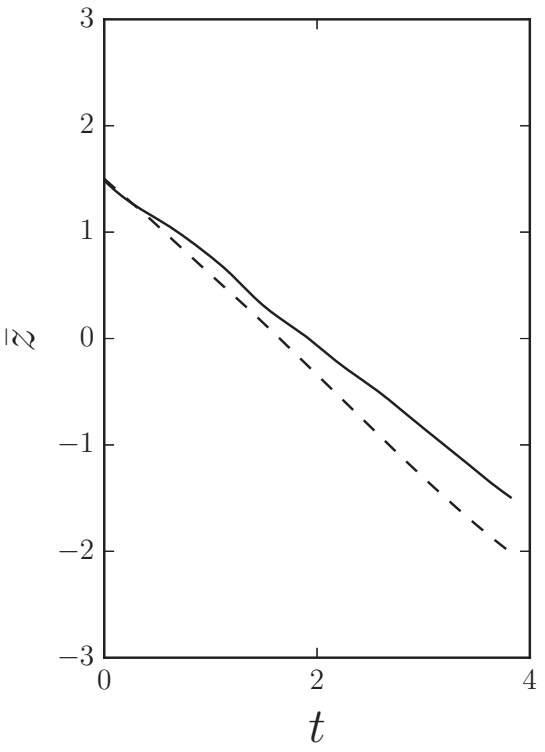

FIG. 3. Vertical position of the centroid of vorticity for the line vortex (solid line) and the vortex pair (dashed line) with constant density.

and (27). Reference to a "vortex pair" implies a simulation initiated with a vortex pair using the initial velocity field given by (24) and (25).

A. $F_r > 1$

Consider the case without stratification by choosing F_r to be infinite. Figure 2 shows contours of vorticity for this case at three time values. The left panels in Fig. 2 show the vortex pair, while the right panels show the line vortex. The parameter values for both cases are the same. The remainder of the results also use these parameter values. Both the vortex pair and the line vortex are released at the same vertical position. Note that light shading in Fig. 2 indicates positive vorticity, while dark shading indicates negative.

The left panels in Fig. 2 show that the vortex pair remains coherent and moves downward, as expected. The right panels show a similar development for the line vortex. The initial vortex line is straight and horizontal but very quickly gets distorted into a "V" shape, as shown in Fig. 2(a). The vortex line "rolls up" and moves downward, finally resembling the vortex pair, as shown in Fig. 2(c).

The vortex pair and line vortex do not reach the same vertical position in Fig. 2(c): the vortex pair has moved farther downward. The location of the vortex is not well defined but may be approximated by the location of the centroid of vorticity, denoted by $\bar{x}$, $\bar{z}$:

$$\bar{z} = \frac{\int z|\eta|^2\, dA}{\int |\eta|^2\, dA}, \quad \bar{x} = \frac{\int x|\eta|^2\, dA}{\int |\eta|^2\, dA},$$

where each integral is performed over the entire domain. These integrals are executed using Gaussian integration with exponential accuracy, and the resulting locations may be any position

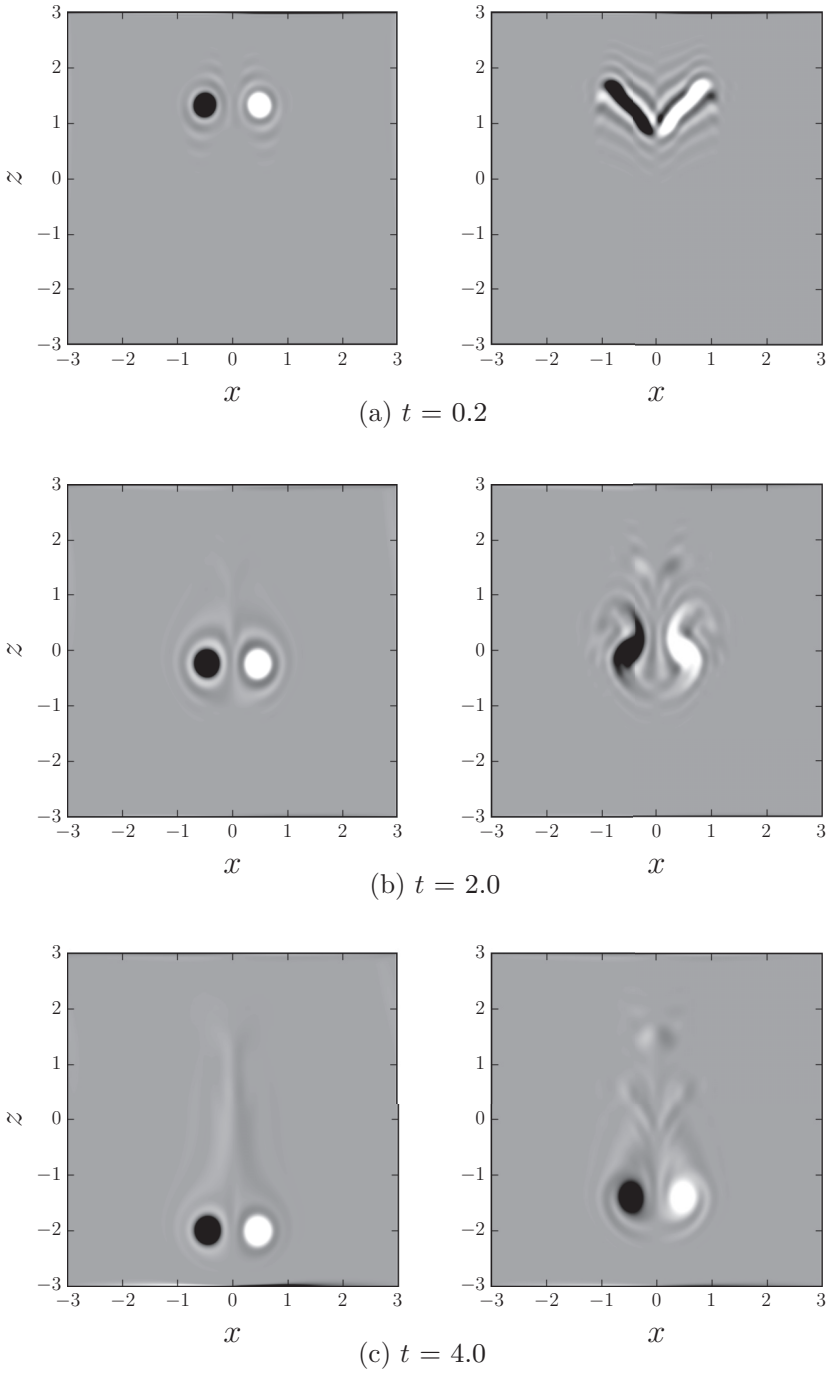

FIG. 4. Contours of vorticity for the vortex pair (left) and the line vortex (right) with $F_r = 4$ (same contour increments as Fig. 2).

(not just a grid-point position). Figure 3 shows the vertical centroid position versus time for both the vortex pair (dashed line) and the line vortex (solid line) for the case of Fig. 2. The slope of the line is the vertical speed of the vortices, which for the vortex pair gives an average speed of 0.93.

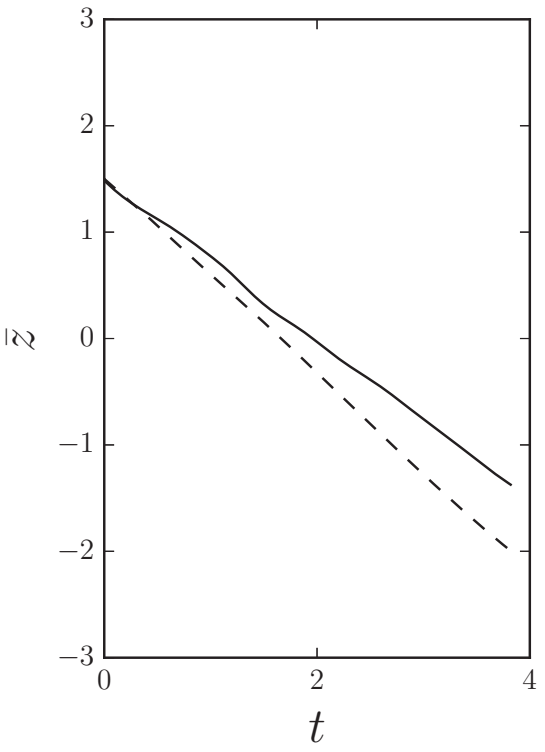

FIG. 5. Vertical position of the centroid of vorticity for the line vortex (solid line) and the vortex pair (dashed line) with $F_r = 4$.

The velocity scale is chosen here to be the induced velocity W_0, hence the dimensionless vertical velocity of the vortex pair is expected to be approximately unity, and this computational value of 0.93 approximately matches the expected value. If the flow was irrotational and the initial conditions were those of a potential flow vortex, then the vertical velocity should be exactly unity.

The vertical position of the line vortex in Fig. 3 experiences some weak oscillations early in the motion, $t < 2.5$. The vortex line is experiencing much of the roll-up process during this time and appears to decrease in speed, while later ($t > 3$) the speed is approximately constant. For this later period ($3 < t < 4$), the average speed is 0.79, slower than the vortex pair. This slower descent speed may be due to the roll-up process of the line vortex, which apparently continues throughout the descent. Again, some of the differences in ascent speed can be attributed to the use of Gaussian vortices, not potential flow vortices.

Now choose the stratification to be nonzero. Contours of vorticity with $F_r = 4$ are shown in Fig. 4. The left and right panels in Fig. 4 are again the vortex pair case and the line vortex case, respectively. The contours for the vortex pair case do not show any wave-making structures, matching the previous results of Garten *et al.* [1]. The contours for the line vortex case also do not show wave making. Comparing Fig. 4 to Fig. 2, the results for the present $F_r = 4$ are very similar to the constant density case for both vortex pair and line vortex. Furthermore, the vertical position of the vortices shown in Fig. 4 is very close to that of Fig. 2, as shown in Fig. 5.

For such large Froude numbers, the centrifugal acceleration of the spinning fluid is stronger than the buoyancy effects, and hence the advection dominates. For such cases the temperature in the core of the vortices becomes mixed very quickly, and each vortex forms into an isolated uniform-temperature entity. The stratification outside of the core is still mostly vertical, but this is unaffected by the overturning motion, which is restricted to the core. As the vortex loses energy by viscous

dissipation, the effective Froude number would seem to decrease; however, waves still do not form due to the well-mixed interior. The opportunity for the flow to make waves is lost once the mixing occurs.

Garten *et al.* [1] used the vorticity equation to demonstrate that vorticity is created baroclinicly in stratified flow, and as a result the vortex pair leaves behind a vortex wake. The vorticity equation (18) for the constant-density case in Fig. 2 reduces to

$$\frac{D\eta}{Dt} = \frac{1}{R_e}\nabla^2\eta, \tag{29}$$

e.g., the baroclinic source term in (18) is zero. This means that there is no significant vorticity wake above the vortex pair, as can be seen in the left panels in Fig. 2. In contrast, the stratified case with $F_r = 4$ in Fig. 4 does have baroclinic vorticity creation, and the vortex pair does indeed leave a vorticity wake, as can be seen in the left panels of Fig. 4. The relationship between the baroclinic source term in the vorticity equation and the vorticity wake has also been discussed by Ortiz *et al.* [23] and Ravichandran *et al.* [22].

However, the line vortex treated here has a significant vorticity wake even without stratification, as can be seen in the right panels in Fig. 2. Baroclinic vorticity generation is zero for this case, thus this wake is due to the advection effects that occur during roll-up. The wake is also present with stratification, as in the right panels of Fig. 4, which has $F_r = 4$. The wake is somewhat stronger with stratification, but the advection effect remains and the presence of this wake behind the rolling up vortex line is due to both advection effects and baroclinic vorticity creation.

B. $F_r < 1$

With $F_r < 1$, Garten *et al.* [1] predict wave-making behavior, but they considered only a vortex pair. The present results with $F_r = 0.5$ for both the vortex pair and the line vortex are shown in Figs. 6 and 7, again using contours of vorticity. The three panels in Fig. 6 are a sequence of time values for the early part of a simulation, while Fig. 7 are later time values.

The sequence for the vortex pair (left panels) shows that the vortex core remains intact for the early times of Fig. 6, but the vertical position does not change significantly from its initial value of $z = 0$ while the horizontal position does change. However, the vorticity field is much more complex with $F_r = 0.5$ than before. Complex bands of vorticity have appeared surrounding the original vortices, in contrast to the $F_r = \infty$ case in Fig. 2, which does not develop such bands. With $F_r = 0.5$ the structures become increasingly complex, with regions of positive and negative vorticity intermixed. This evolution matches that of Garten *et al.* [1].

The right panels show the evolution of the line vortex. The results for the line vortex are significantly different than the vortex pair with $F_r = 0.5$. The roll-up process appears to begin as before and the core vortex begins to form, as shown in Fig. 6(a). But the core does not mature, and by $t = 1.0$ in Fig. 6(b), each side does not have a single vortex core. Instead each side appears to have two cores, and by $t = 2.0$ there are multiple vortex structures on each side, shown in Fig. 6(c). In contrast, the vortex pair during this time still retains the structure of a single vortex on each side.

Later in the simulation, the vortex pair also disintegrates, as shown in Fig. 7. The disintegration of the vortex pair is different than the vortex line in that there remain regions of intense vorticity, presumably the remnants of the original vortices. The line vortex does not retain such regions.

The centroid of vorticity is shown in Figs. 8 and 9 for $F_r = 0.5$. Importantly, the vertical position of the vortices (Fig. 8) for both cases does not change significantly with time, a characteristic of the wave-making behavior regime. Note that the vertical position of the line vortex is very close to the vertical position of the vortex pair (Fig. 8). In contrast, the horizontal position of the vortex pair is much different (Fig. 9). The vortex pair retains a strong core, as can be seen in Fig. 6, and the cores drift outward from the original positions. The vortex line disintegrates faster and does not retain a single coherent core.

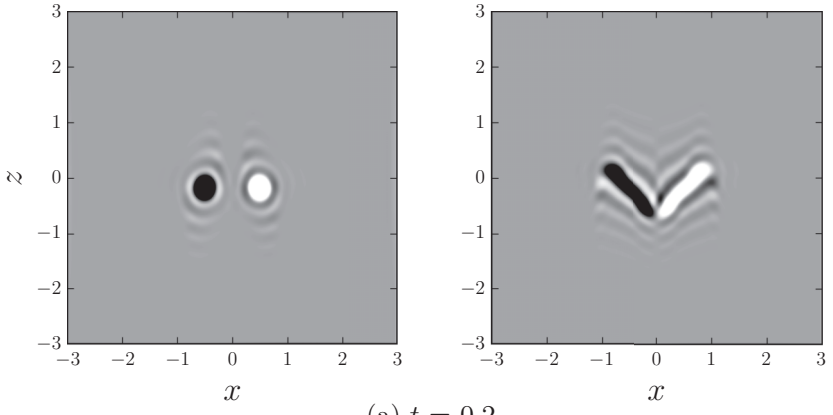

(a) $t = 0.2$

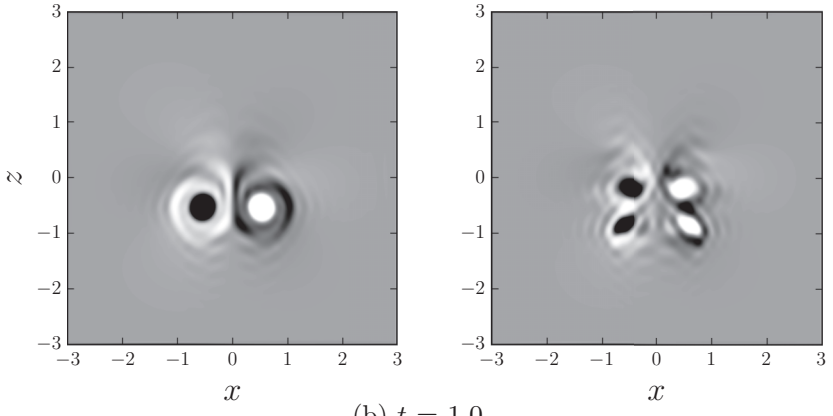

(b) $t = 1.0$

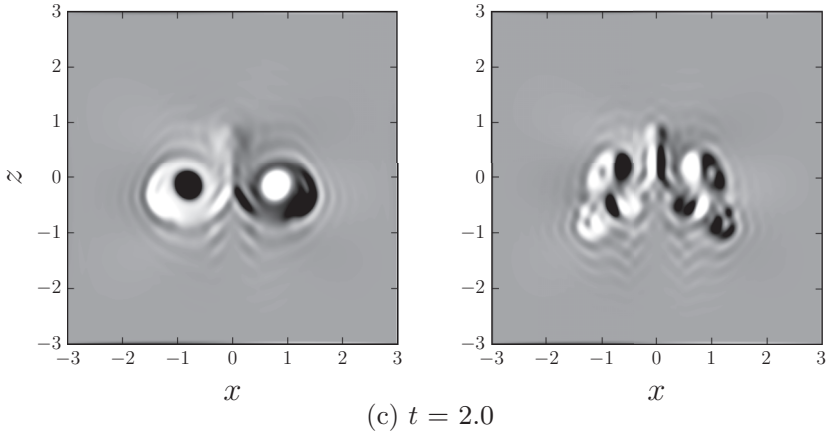

(c) $t = 2.0$

FIG. 6. Contours of vorticity for the vortex pair (left) and the line vortex (right) with $F_r = 0.5$ for early times (same contour increments as Fig. 2).

Note that the simulations allow asymmetry about the centerline; however, the results retain symmetry for both the vortex pair and line vortex for most of the simulations. No noise or other disturbance has been introduced.

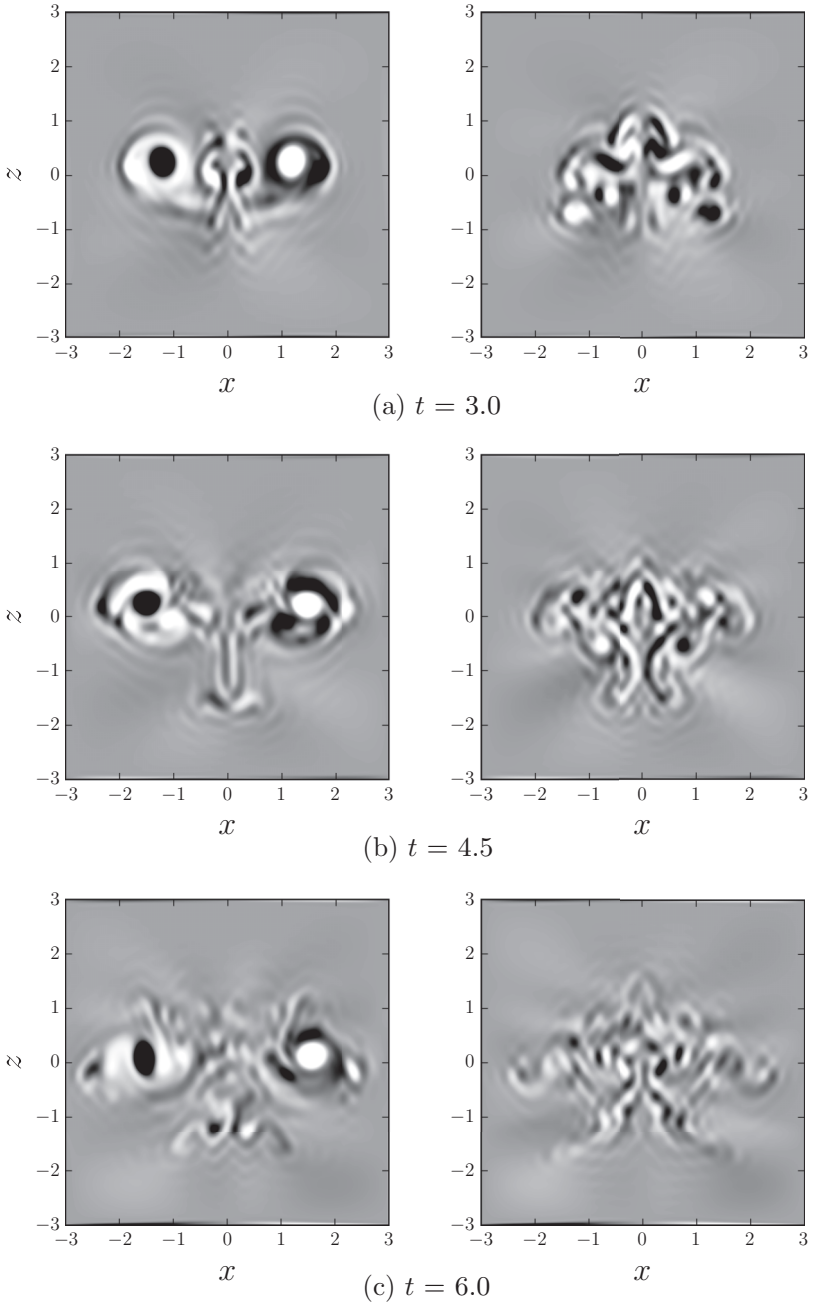

FIG. 7. Contours of vorticity for the vortex pair (left) and the line vortex (right) with $F_r = 0.5$ for later times (same contour increments as Fig. 2).

Results for a lower Froude number, $F_r = 0.1$, are shown in Fig. 10, again for three time values (different times than before). These contours of vorticity show that for both the vortex pair and the line vortex, elongated structures are radiating outward from the original localized vortex flow, growing farther outward with time. As famously discussed by Mowbray and Rarity [31,32], a local disturbance in a stratified fluid will create lines of constant phase that are radial. Furthermore,

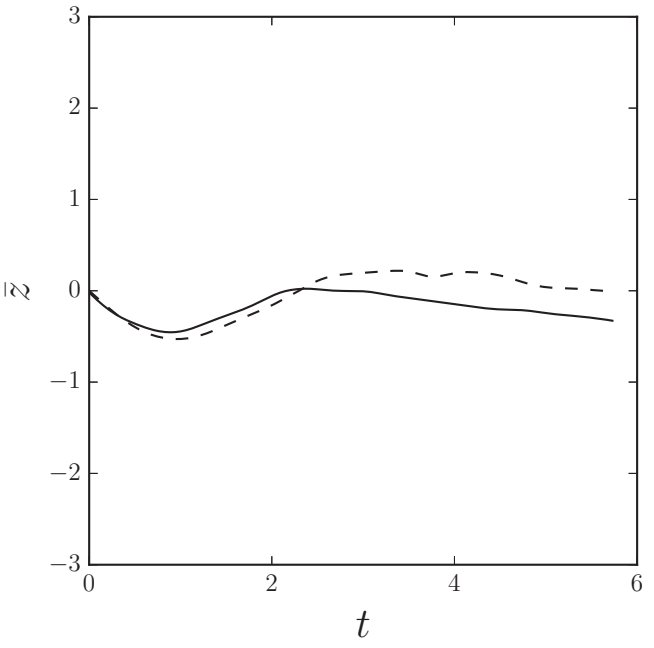

FIG. 8. Vertical position of the centroid of vorticity for the line vortex (solid line) and the vortex pair (dashed line) with $F_r = 0.5$.

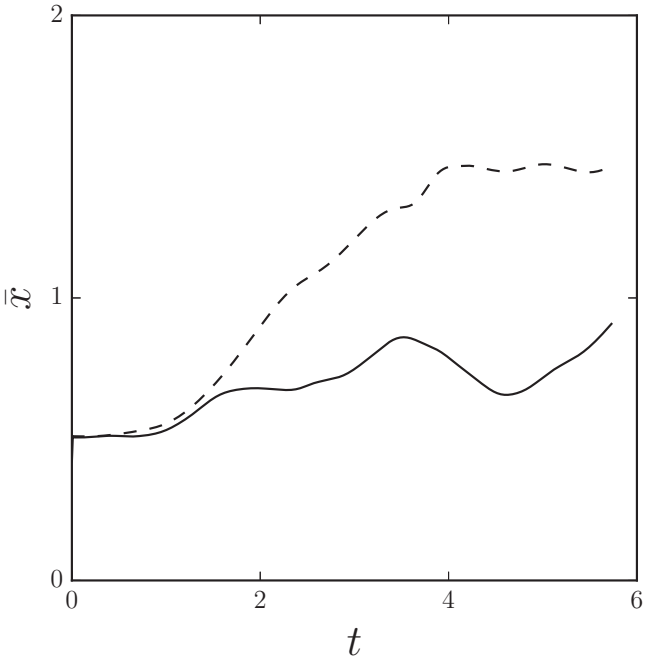

FIG. 9. Horizontal position of the centroid of vorticity for the line vortex (solid line) and the vortex pair (dashed line) for the right side of the domain with $F_r = 0.5$.

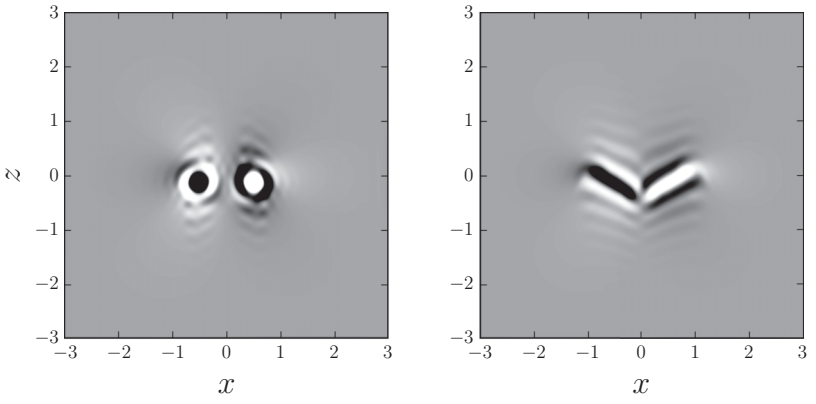

(a) $t = 0.2$

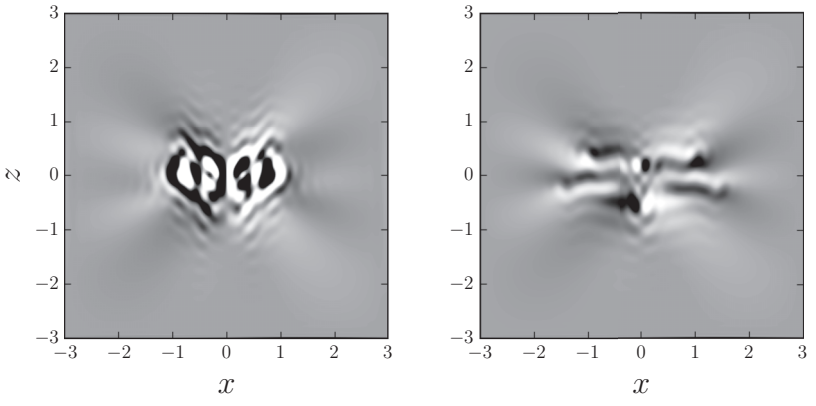

(b) $t = 0.7$

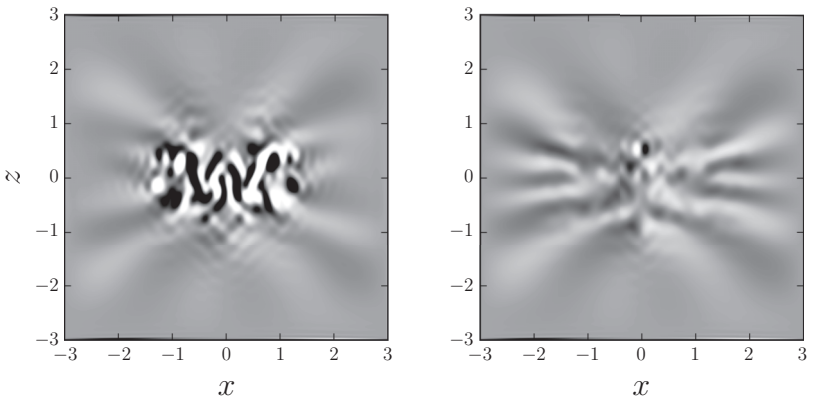

(b) $t = 1.4$

FIG. 10. Contours of vorticity for the vortex pair (left) and the line vortex (right) with $F_r = 0.1$ (same contour increments as Fig. 2).

these radial phase lines are the direction of energy propagation of internal waves. Clearly the structures that are forming in Fig. 10 are precisely these internal wave phase lines. The number of structures is increasing with time for both the vortex pair (left) and the line vortex (right) in

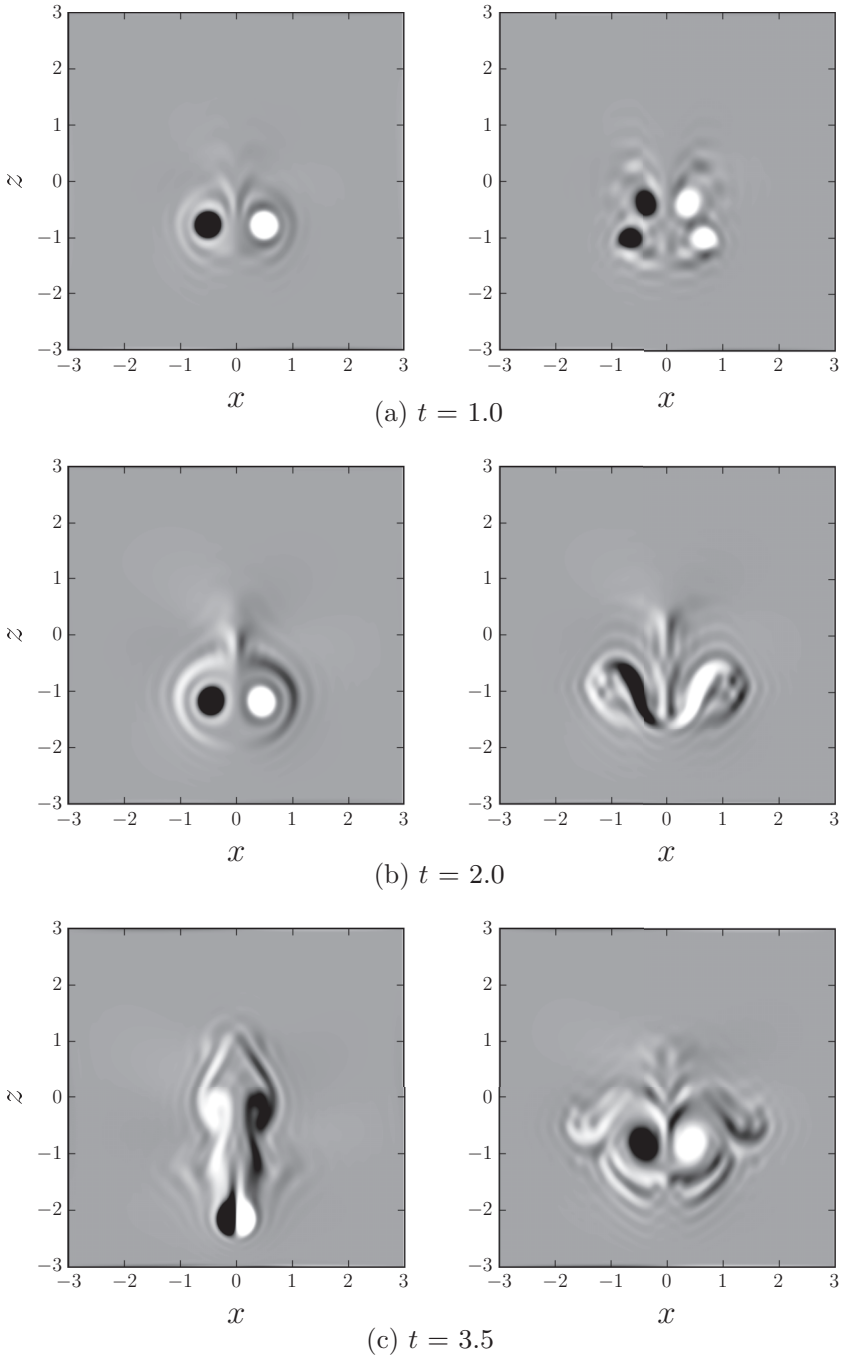

FIG. 11. Contours of vorticity for the vortex pair (left) and the line vortex (right) with $F_r = 1.0$ (same contour increments as Fig. 2).

Fig. 10. This fact suggests that the core flow is experiencing a broader spectrum of frequencies with time.

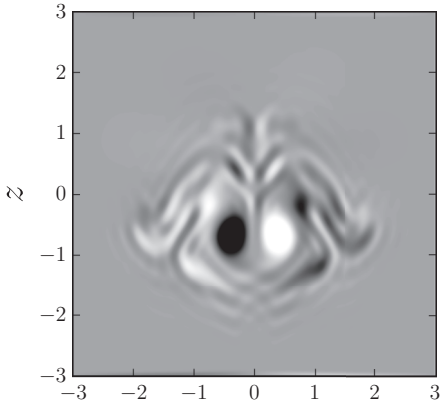

(a) $t = 4.5$

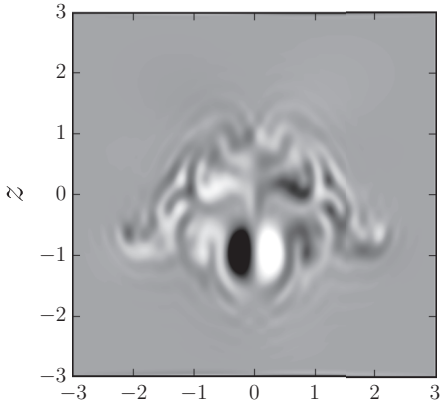

(b) $t = 5.5$

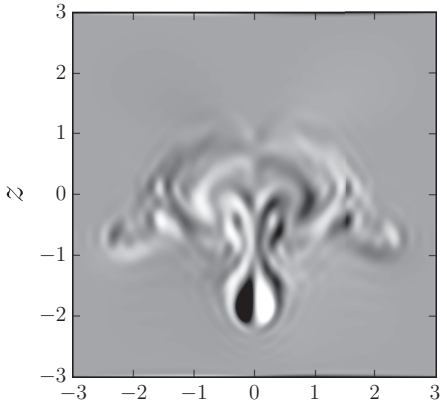

(c) $t = 6.5$

FIG. 12. Contours of vorticity for the line vortex with $F_r = 1.0$ for later times (same contour increments as Fig. 2).

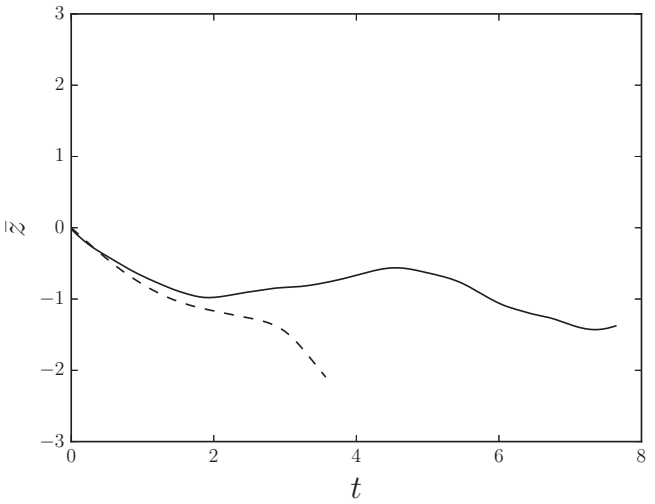

FIG. 13. Vertical position of the centroid of vorticity for the line vortex (solid line) and the vortex pair (dashed line) with $F_r = 1$.

These $F_r = 0.1$ results indicate that the vortices disintegrate at low Froude numbers by creating internal waves, as suggested by Garten *et al.* [1]. With $F_r = 0.5$ the flow does not show such distinct internal wave structures; however, the flow remains symmetric about the centerline of the domain, unlike a turbulent flow, suggesting that the behavior is still related to internal waves.

C. The transitional F_r

Garten *et al.* [1] quote $F_r = 1$ as the transitional value, with $F_r < 1$ being the buoyancy-dominated or wave-making regime. This result was apparently based purely on the flow patterns that emerge during the simulations at different F_r, with all cases initialized using a vortex pair. The present results generally agree with this transitional value for the vortex pair, although the transition between regimes does not seem to be a sharp change in behavior.

Figure 11 provides contours of vorticity for this transitional value of $F_r = 1$ for both vortex pair and the line vortex. The left panels show that the vortex pair maintains its form and propagates downward. No significant internal waves are created. The vortices move closer together as they move downward, as can be seen in Fig. 11(c). This feature was present in the simulations of Garten *et al.* [1] and others.

The right panels in Fig. 11 are the line vortex case. The line vortex begins to roll up and form vortices that are similar to the vortex pair but do not move downward like the vortex pair. Furthermore, the rolled-up vortices are surrounded by bands of positive and negative vorticity that are not present with the vortex pair. The line vortex is still within the wave-making regime at this Froude number.

Figure 12 shows later time values in the evolution of the line vortex. The vortex pair has already reached the bottom of the computational domain and is not shown. Figure 12 shows that the line vortex continues to generate a complex pattern of vorticity surrounding the remnants of the line vortex, but then finally creates a much smaller structure that resembles the vortex pair. This structure then propagates downward, finally impinging on the computational boundary.

Figures 13 and 14 show the evolution of the position of the centroid of vorticity for $F_r = 1$, both vortex pair and line vortex. This vorticity centroid has been found to track the obvious position of the vortex pair when the vortices are coherent. The vertical position of the vortex pair in Fig. 13 (dashed line) shows that the vortex pair reaches a stage around $t \approx 3$ where it moves downward much faster.

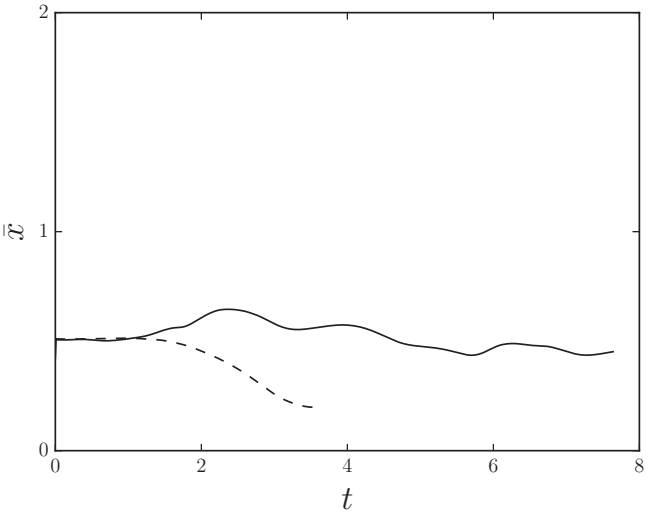

FIG. 14. Horizontal position of the centroid of vorticity for the line vortex (solid line) and the vortex pair (dashed line) for the right side of the domain with $F_r = 1$.

The distance between the vortices is decreasing near $t \approx 3$, as can be seen in the horizontal position of the right-hand vortex in Fig. 14, hence the speed increase appears to be related to this feature. This scenario has been reported previously [1,22,23]. The downward motion is due to the pressure distribution that develops around the volume of well-mixed fluid inside the vortex pair, similar to the constant-density case. The horizontal drift is due to the creation of opposite-signed vorticity at the edge of each original vortex that results in a baroclinic torque. This recently created vorticity is visible in Fig. 12 and is particularly visible in the middle frame ($t = 2.0$).

The solid line in Fig. 13 is quite different, indicating that the vortex line does not propagate downward in the same manner. This fact may not seem consistent with Fig. 12, which does show a small vortex pair propagating to the bottom of the computational domain. However, the wake of this vortex pair has strong levels of vorticity, and thus the centroid of vorticity is in a different position than this small but visible vortex pair.

It may be argued that the line vortex is not really in the wave-making regime with $F_r = 1$, since it finally created a vortex pair structure. However, the vortex pair with $F_r < 1$ will also generate waves and then finally release a smaller vortex pair structure in this same manner, despite being clearly in the wave-making regime of Garten *et al.* [1]. Consider the evolution of the vortex pair with $F_r = 0.8$ in Fig. 15. The vortex pair structure for the line vortex in Fig. 12 is very similar to that of Fig. 15 and must also be considered within the wave-making regime. Thus the final appearance of a smaller vortex pair cannot be used to define the regimes of motion.

The characteristics of the wave-making regime are (1) the original vortex structure does not propagate vertically and (2) complex patterns of vorticity form around the original vortex structure. These behavior patterns are strikingly different when F_r is much different than unity. However, near the transition value of F_r, the vorticity patterns are not much different, and the transition between the two regimes appears to be gradual, making the transitional F_r difficult to determine. The position of the vorticity centroid appears to be the best measure of transition, although still imperfect.

Figure 16 shows the vertical position of the centroid of vorticity for the line vortex (solid lines) with $1 \leqslant F_r \leqslant 2$, along with $F_r = 4$. The $F_r = 4$ case closely matches the constant density case, where waves cannot be generated, and thus $F_r = 4$ is clearly not in the wave-making regime. The solid lines with $F_r = 1, 2$ are labeled, while the solid lines between these two have F_r incremented by

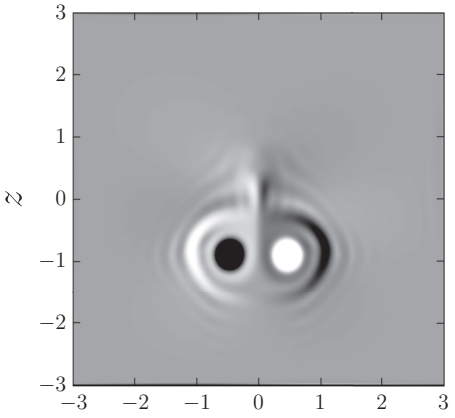

(a) $t = 2.0$

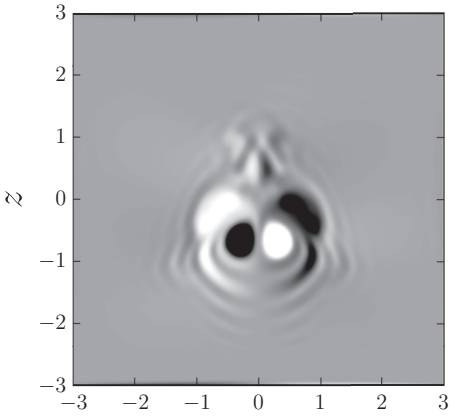

(b) $t = 3.0$

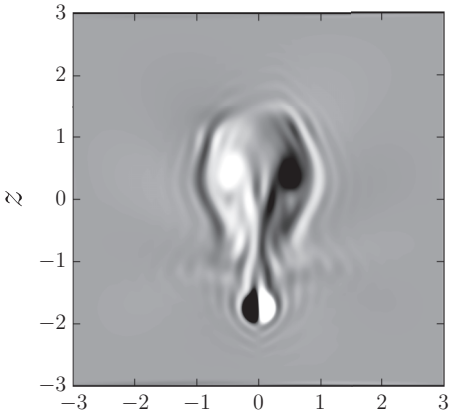

(c) $t = 4.0$

FIG. 15. Contours of vorticity for the vortex pair with $F_r = 0.8$ (same contour increments as Fig. 2).

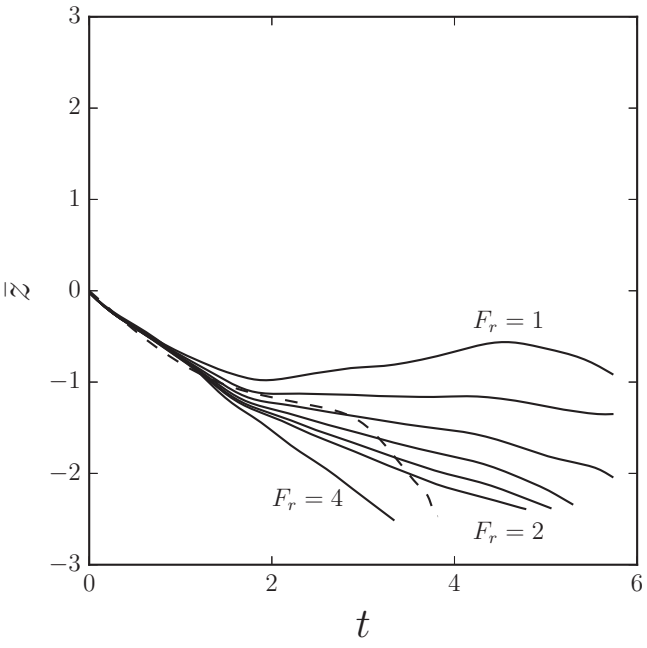

FIG. 16. Vertical position of the centroid of vorticity for the line vortex (solid lines) for cases with $1 \leqslant F_r \leqslant 2$, as well as the case with $F_r = 4$. The dashed line is the vortex pair with $F_r = 1$.

0.2. Clearly there is a gradual transition in behavior with increasing F_r. With $F_r = 2$, the vortex line moves downward similar to the $F_r = 4$, case, although more slowly, and thus the $F_r = 2$ case might not be in the wave-making regime. With $F_r = 1$, the centroid position does not move downward, strongly suggesting that $F_r = 1$ is well within the wave-making regime with the line vortex. The vortex pair with $F_r = 1$ is also shown in Fig. 16 with a dashed line and indicates much different behavior. Overall, Fig. 16 indicates that the transition value is closer to $F_r = 2$ for the line vortex, compared to $F_r = 1$ for the vortex pair.

V. CONCLUSIONS

Previous computational results indicate that vortices in stratified flow at large F_r will remain coherent and behave in a manner that matches the flow with constant density. Vortices with small F_r act differently, creating a pattern of internal waves. However, this wave making occurs soon after initiation, before mixing eliminates any significant stratification. Previous results initiated the flow with a laminar vortex pair, which does not match the manner in which a vortex is formed behind a wing or other lifting surface, where the trailing vorticity is distributed. The roll-up of the distributed vorticity should occur in the presence of stratification.

This process has been treated here with numerical simulations in two dimensions. The initial flow is a horizontal line vortex with constant strength, created with a sequence of Gaussian vortices. This allows the velocity field to evolve along with the density field, as happens in practice. The results show that the distributed vorticity is much more inclined to form internal waves. Previous results indicate that $F_r = 1$ is the transitional value for wave generation; however, here the transitional value has been found to be closer to $F_r = 2$. This transitional value is found using the vertical motion of the vortices: coherent vortices will propagate vertically while wave-generating vortices do not.

[1] J. F. Garten, S. Arendt, D. C. Fritts, and J. Werne, Dynamics of counter-rotating vortex pairs in stratified and sheared environments, J. Fluid Mech. **361**, 189 (1998).
[2] L. Prandtl, Nachr. Ges. Wiss. Goettingen, Math. Phys. Kl. **1918**, 451 (1918).
[3] P. R. Spalart, Airplane trailing vortices, Annu. Rev. Fluid Mech. **30**, 107 (1998).
[4] V. J. Rossow, Lift-generated vortex wakes of subsonic transport aircraft, Prog. Aero. Sci. **35**, 507 (1999).
[5] T. Gerz, F. Holzapfel, and D. Darracq, Commercial aircraft wake vortices, Prog. Aero. Sci. **38**, 181 (2002).
[6] R. Paoli and K. Shariff, Contrail modeling and simulation, Ann. Rev. Fluid Mech. **48**, 393 (2016).
[7] J. Lighthill, *An Informal Introduction to Theoretical Fluid Mechanics* (Cambridge University Press, Cambridge, 1986).
[8] H. Kaden, Aufwicklung einer unstabilen Unstetigkeitsflach, Ing. Arch. **2**, 140 (1931).
[9] J. R. Spreiter and A. H. Sacks, The rolling up of the trailing vortex sheet and its effect on the downwash behind wings, J. Aero. Sci. **18**, 21 (1951).
[10] D. W. Moore and P. G. Saffman, Axial flow in laminar trailing vortices, Proc. Roy. Soc. Lond. **333**, 491 (1973).
[11] A. J. Bilanin and C. D. Donaldson, Estimation of velocities and roll-up in aircraft vortex wakes, J. Aircraft **12**, 578 (1975).
[12] E. Chadwick and T. Rahulan, A theoretical model evaluating leading order vortex decay behind an aircraft, J. Aero. Eng. **225**, 657 (2011).
[13] M. Czech, G. Miller, J. Crouch, and M. Strelets, Predicting the near-field evolution of airplane trailing vortices, CR Phys. **6**, 451 (2005).
[14] P. G. Saffman, The motion of a vortex pair in a stratified atmosphere, Stud. Appl. Math. **51**, 107 (1972).
[15] J. S. Turner, A comparison between buoyant vortex rings and vortex pairs, J. Fluid Mech. **7**, 419 (1960).
[16] F. M. Hill, A numerical study of the descent of a vortex pair in a stably stratified atmosphere, J. Fluid Mech. **71**, 1 (1975).
[17] P. R. Spalart, On the motion of laminar wing wakes in a stratified fluid, J. Fluid Mech. **327**, 139 (1996).
[18] R. E. Robins and D. P. Delisi, Numerical simulations of three-dimensional trailing vortex evolution, AIAA J. **35**, 1552 (1997).
[19] F. Holzapfel and T. Gerz, Two-dimensional wake vortex physics in the stably stratified atmosphere, Aero. Sci. Tech. **3**, 261 (1999).
[20] K. K. Nomura, H. Tsutsui, D. Mahoney, and J. W. Rottman, Short-wavelength instability and decay of a vortex pair in a stratified fluid, J. Fluid Mech. **553**, 283 (2006).
[21] S. C. Crow, Stability theory for a pair of trailing vortices, AIAA J. **8**, 2172 (1970).
[22] S. Ravichandran, H. N. Dixit, and R. Govindarajan, Lift-induced vortex dipole collapse, Phys. Rev. Fluids **2**, 034702 (2017).
[23] S. Ortiz, C. Donnadieu, and J. M. Chomaz, Three-dimensional instabilities and optimal perturbations of a counter-rotating vortex pair in stratified flows, Phys. Fluids **27**, 106603 (2015).
[24] F. B. Lipps and R. S. Hemler, A scale analysis of deep moist convection and some related numerical calculations, J. Atmos. Sci. **39**, 2192 (1982).
[25] J. P. Boyd, *Chebyshev and Fourier Spectral Methods* (Dover, New York, 2001).
[26] G. E. Karniadakis, M. Israeli, and S. A. Orszag, High-order splitting methods for the incompressible Navier-Stokes equations, J. Comput. Phys. **97**, 414 (1991).
[27] D. N. Slinn and J. J. Riley, A model for the simulation of turbulent boundary layers in an incompressible stratified flow, J. Comp. Phys. **144**, 550 (1998).
[28] H. Vandeven, Family of spectral filters for discontinuous problems, J. Sci. Comput. **6**, 159 (1991).
[29] A. Betz, Behavior of vortex systems, Z. Angw. Math. Mech. **12**, 164 (1932).
[30] W. R. C. Phillips, The turbulent trailing vortex during roll-up, J. Fluid Mech. **105**, 451 (1995).
[31] D. E. Mowbray and B. S. Rarity, The internal wave pattern produced by a sphere moving vertically in a density stratified liquid, J. Fluid Mech. **30**, 489 (1967).
[32] D. E. Mowbray and B. S. Rarity, A theoretical and experimental investigation of the phase configuration of internal waves of small amplitude in a density stratified liquid, J. Fluid Mech. **28**, 1 (1967).